*First publ. in: Applied Physics A 55 (1992), pp. 482-488*

# Generation Mechanism for Coherent LO Phonons in Surface-Space-Charge Fields of III–V-Compounds

**T. Pfeifer, T. Dekorsy, W. Kütt, and H. Kurz**

Institute of Semiconductor Electronics, RWTH Aachen, W-5100 Aachen, Fed. Rep. Germany (Fax: +49-241/86165)

**Abstract.** We report on details of coherent LO phonon generation in surface-space-charge regions of III–V-compounds by optical injection of free carriers with laser pulses of 50 fs duration at 2 eV. Both the dynamics of the transient surface field, as well as the coherent lattice vibration, are measured via electro-optic sampling techniques under different experimental conditions. The driving force for the coherent phonon vibration is the sudden depolarization of the crystal lattice due to ultrafast screening of the intrinsic electrical surface field by photoexcited free carriers.

**PACS:** 78.47.+p, 42.65.Re, 63.20.−e

Since the invention of the CPM ring dye laser, pump-probe techniques have widely been used to study relaxation of nonequilibria in condensed matter down to the subpicosecond time regime [1, 2]. In many of these experiments periodic modulations of transmission or reflectivity changes are observed [3–8]. They are related to coherent lattice vibrations, modifying the optical dielectric functions. First theoretical explanations of this phenomenon invoked impulsive stimulated Raman scattering (ISRS) [9]. There, the coherent phonons are driven by the difference-frequency of two laser fields contained within an ultrashort laser pulse of sufficient spectral bandwidth. More recently, a displacive excitation mechanism of coherent phonons (DECP) has been discussed. In this case the phonon amplitude is driven by sudden perturbations of the electronic system [10]. Anisotropic hole distributions constitute the driving force for coherent phonons in Ge [11].

A completely different excitation mechanism is found in polar III–V-materials. Optical injection of free carriers by ultrashort laser pulses leads to an ultrafast depolarization of the crystal lattice by screening the electrical field in the surface-space-charge region [7]. This process can be so fast, that coherent longitudinal lattice vibrations are launched.

In this paper, a detailed investigation of the generation mechanism for coherent LO phonons in surface-space-charge regions of III–V-compounds will be presented. In Sect. 1, the classical equation of motion for the harmonic oscillator is presented, including specific driving force terms for coherent longitudinal optical phonons. In Sect. 2 the experimental apparatus for performing time-resolved pump-probe experiments is outlined. We use a reflective electro-optic detection geometry (time resolved REOS technique [12, 13]), which is sensitive to longitudinal electrical field changes. Detailed studies of the generation process for coherent LO phonons in surface-space-charge fields are presented in Sect. 3. These experiments confirm that coherent LO phonons in surface-space-charge regions are launched by an ultrafast longitudinal depolarization of the crystal lattice induced by the screening of the surface field via the photoexcited free carriers.

## 1 Driving Forces for Coherent LO Phonons

The most distinct feature of a coherent vibration is the fixed phase relationship among individual modes. Under this condition the amplitude of the coherent oscillation $Q(t)$ can be described by the classical equation of motion of a harmonic oscillator [14]:

$$\mu\left(\frac{\partial^2 Q_j(t)}{\partial t^2} + 2\Gamma\frac{\partial Q_j(t)}{\partial t} + \omega_{\mathrm{LO}}^2 Q_j(t)\right) = F_j^{Q_j(t)}. \qquad (1)$$

where $\mu$ is the reduced lattice mass, $\Gamma = T_2^{-1}$ the dephasing rate, $\omega_{\mathrm{LO}}$ the LO phonon frequency, and $F_j^{Q_j(t)}$ the driving force. In non-centrosymmetric polar semiconductors any nonlinear polarization with a dominant frequency component at $\omega_{\mathrm{LO}} = (E_k - E_l)/\hbar$ can resonantly drive LO phonons. Thus, in addition to the atomic displacement Raman tensor, the driving force contains contributions, that are associated with the longitudinal component of a nonlinear polarization $P_j^{NL}$ [14]:

$$F_j^{Q_j(t)} = R_{jkl}E_kE_l - \frac{e^*}{\varepsilon_{(\infty)}\varepsilon_0}P_j^{NL}(t), \qquad (2)$$

where $e^*$ is the effective lattice charge, $\varepsilon_{(\infty)}$ the high-frequency dielectric constant, $\varepsilon_0$ the vacuum permittivity, and $E_k$, $E_l$ pump-field components. The indices $j$, $k$, $l$ denote the Cartesian coordinates, where $j$ is the $x = (100)$ direction of the LO phonon displacement normal to the surface and $k, l$ denote the $y = (010)$ or $z = (001)$ directions. The atomic-displacement Raman tensor $R_{jkl}$ determines the coupling via deformation potential interactions. The nonlinear polarization $p^{NL}$ is composed of

$$P_j^{NL}(t) = \chi^{(2)}_{jkl} E_k E_l + \chi^{(3)}_{jklm} E_k E_l E_m + \int_{-\infty}^{t} J_j(t')dt' \,, \quad (3)$$

where $\chi^{(2)}_{jkl}$ and $\chi^{(3)}_{jklm}$ are the second- and third-order nonlinear susceptibilities, and $J_j(t)$ is a current associated with the drift of photoexcited carriers in surface-space-charge fields. The second-order term describes the instantaneous electro-optic coupling, set up by difference-frequency mixing of the laser fields. It has the same symmetry as the atomic-displacement Raman term $R_{jkl}$ ($\neq 0$, only for $j \neq k \neq l$), but is of opposite sign. Both terms form an effective Raman tensor in polar materials [14]:

$$\bar{R}_{jkl} = R_{jkl} - \frac{e^*}{\varepsilon_{(\infty)}\varepsilon_0} \chi^{(2)}_{jkl} \,. \quad (4)$$

In addition, third- and higher-order nonlinear polarizations have to be taken into account, when strong femtosecond laser pulses excite the surface. For the third-order term to be effective, symmetry selection rules for elements of the $\bar{4}3m$ group require a third field (e.g., $E_m$) in (100)-direction [15].

Coherent LO phonon generation via ultrafast photocurrents can be understood in a simple, but very illustrative picture: In polar semiconductors the conduction and valence bands are bent at the surface (Fig. la), because of Fermi-level pinning at charged surface states [16]. This results in a static electrical field perpendicular to the surface

$$E_j(x) = E_S\left(1 - \frac{1}{w}x\right) \qquad (0 \leq x \leq w) \quad (5)$$

where $x$ denotes the $j = (100)$ direction, $E_S$ the static electric surface field, and $w$ the depth of the depletion zone

$$E_S = \sqrt{\frac{2qN_D}{\varepsilon_0\varepsilon_{(0)}}\left(V_{bi} - U - \frac{kT}{q}\right)} \,,$$
$$w = \sqrt{\frac{2\varepsilon_0\varepsilon_{(0)}}{qN_D}\left(V_{bi} - U - \frac{kT}{q}\right)} \quad (6)$$

with $q$ the electron charge, $\varepsilon_{(0)}$ the static dielectric constant, and $V_{bi}$ the built-in potential, which is 0.7 eV and 0.5 eV in $n$- and $p$-doped GaAs, respectively. The term $kT/q$ is negligible at room temperature. Thus, the static electric surface field $E_S$ and the depth of the surface space-charge zone $w$ can be controlled by the doping level $N_D$ and/or by an externally applied bias voltage $U$. In any case, illumination of the surface will give rise to a screening of the surface field depending on the excitation density. Figure lb illustrates the case of strong illumination, leading to near-flat band conditions at the end of the pump pulse duration.

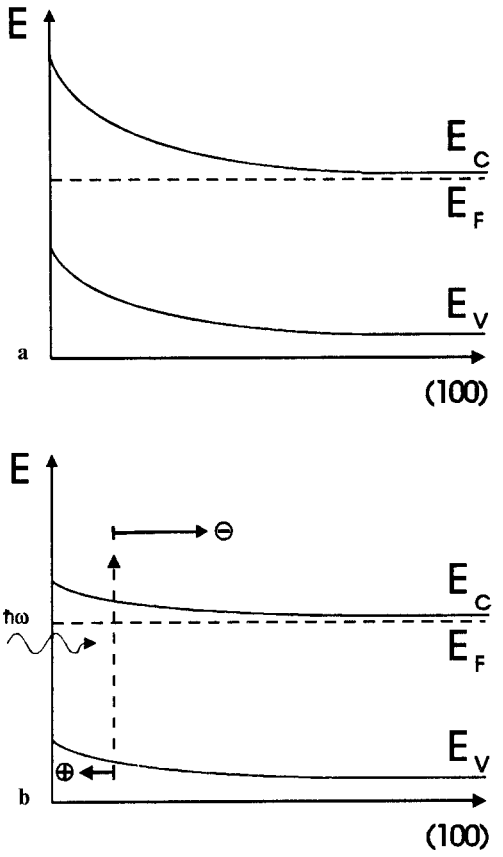


**Fig. 1.** **a** Initial band ending at the surface of a $n$-doped polar semiconductor, and **b** near-flat-band conditions due to charge separation by drift and diffusion processes after optical injection of free carriers

The static electrical field polarizes the crystal lattice in the surface-space-charge region giving an atomic displacement [17]

$$Q^s = \frac{\varepsilon_0(\varepsilon_{(0)} - \varepsilon_{(\infty)})}{Ne^*} E_S \,, \quad (7)$$

where $N$ is the density of pairs of atoms per unit cell, and $E_S$ the electrical surface field as defined above. For $n$-type GaAs of a typical doping level of $N_D = 5 \times 10^{17}\,\mathrm{cm}^{-3}$ the surface field is $E_S = 310\,\mathrm{kV/cm}$, leading to an atomic displacement of $Q^s = 8 \times 10^{-3}$ Å.

Figure 2 shows a simple, one-dimensional illustration of this situation. The crystal lattice is represented by a linear chain of coupled, oppositely charged ions. When a static electric field is applied along the chain, the atoms will follow in accordance to their charge, thus deforming the chain longitudinally (Fig. 2b). Certainly the atoms will relax to a new equilibrium position (Fig. 2a), when the electric field is switched off. If this process is very fast, the

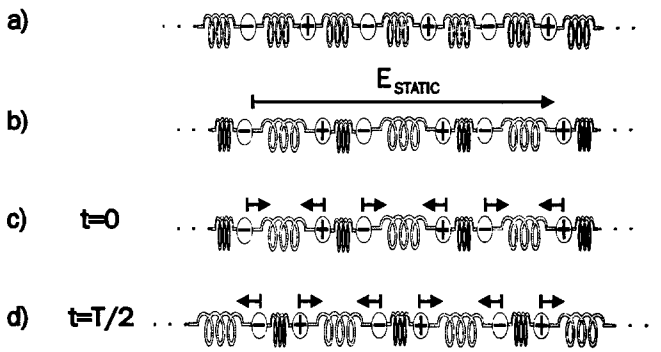


**Fig. 2. a** Simple model of a linear chain composed of coupled, oppositely charged atoms, longitudinally deformed by a static electric field, **b**. Rapid decrease of the field at $t = 0$ launches longitudinal oscillations, as illustrated in **c** and **d** for different times $t$ ($T/2$ is equivalent to a half period)

atoms will overshoot their equilibrium position launching a longitudinal oscillation of the chain. This is illustrated in Figs. 2c, d for different times $t$. At $t = 0$ the electric field is switched off (Fig. 2c) and Fig. 2d depicts the situation at half of the oscillation period, $t = T/2$. The atoms will oscillate against each other in a longitudinal mode with the same phase throughout the whole irradiated volume. The temporal evolution of the displacement of the positively and negatively charged atoms $Q_{\pm}(t)$ can be described by $Q_{\pm}(t) = Q_0 \cos(\omega_{LO} t + \varphi_{\pm})$, where $\varphi_{\pm} = 0, \pi$, denotes the initial phase, and $Q_0$ the amplitude of the oscillation. It should be noted that the amplitude is determined by both the static atomic displacement as well as the speed of depolarization, which determines the driving force.

At the surface of semiconductors the surface-space-charge fields are modified ("switched off") by optical injection of free carriers. These photocurrents give an additional polarization $P_j(t) = \int J_j(t')\,dt'$. The central part of our experiments is concerned with the question, whether the rise time of this longitudinal polarization is sufficiently short to launch coherent LO phonons.

## 2 Electro-Optic Detection

The longitudinal field changes associated with the charge separation and the coherent LO phonons deform the optical indicatrix of (100)-oriented III–V-compounds via the electro-optic effect (Fig. 3a). The index of refraction is modified according to

$$n(\gamma) = n_0 + \frac{1}{2} n_0^3 r_{41} \Delta E_{(100)} \sin(2\gamma) \tag{8}$$

where $n_0$ is the isotropic index of refraction, $r_{41}$ the electro-optic coefficient, $\Delta E_{(100)}$ the electrical field in (100) direction, and $\gamma$ is the angle between the polarization of the probe beam (in the (100) plane) and the (001) crystal axis. Neglecting contributions of changes in the absorption coefficient, the reflectivity change is

$$\frac{\Delta R}{R_0} = \frac{1}{R_0} \frac{\partial R}{\partial n} \Delta n, \tag{9}$$

where $R_0$ is the unperturbed reflectivity.

In order to detect these field-induced reflectivity changes, highly sensitive detection schemes have to be applied. Ultrashort laser pulses of 50 fs duration and 2 eV energy derived directly from a dispersion-compensated CPM-ring-dye laser, are split in a conventional pump-probe set-up into a strong pump-pulse and an orthogonally polarized weak probe pulse. After traversing different paths, the two beams are focused on the sample. The probe pulse is polarized parallel to the $(0\bar{1}0)$ crystal axis. The reflected part of the probe beam is split via a polarizing cube beam splitter into its orthogonal components along the $(0\bar{1}1)$ and $(0\bar{1}\bar{1})$ directions. The difference in reflectivity change of the two orthogonal components is proportional to the electric field changes in (100)-direction

$$\frac{\Delta R_{eo}}{R_0}(t) = \frac{R_{(0\bar{1}1)}(t) - R_{(0\bar{1}\bar{1})}(t)}{R_0} \approx \frac{4 n_0^3 r_{41}}{n_0^2 - 1} \Delta E_{(100)}(t) \,. \tag{10}$$

The experimental set-up of this reflective, electro-optic sampling (REOS) technique [12, 13] is exhibited in Fig. 3b.

Time-resolved measurements are accomplished by scanning the optical path difference between the pump and probe beams by a retroreflector mounted on a shaker-scanner driven at 50–200 Hz. Maximum time delays are 2–20 ps, depending on the shaker frequency. The difference signal is directly fed into a specially developed data-acquisition system, comprising a high-speed data-acquisition unit and a 4 MHz 12-bit AD converter [18]. With this "fast-scan" technique, detectable signal changes are a few $10^{-7}$ when averaging over $10^5$ scans within 10 min.

Additionally, a time derivative technique has been used [19]. In this case, the shaker, driven at a frequency of $\nu_S = 600$ Hz, modulates the time delay with a small amplitude of less than $\Delta t_0 = 20$ fs. The recorded signal $\Delta R$ of this

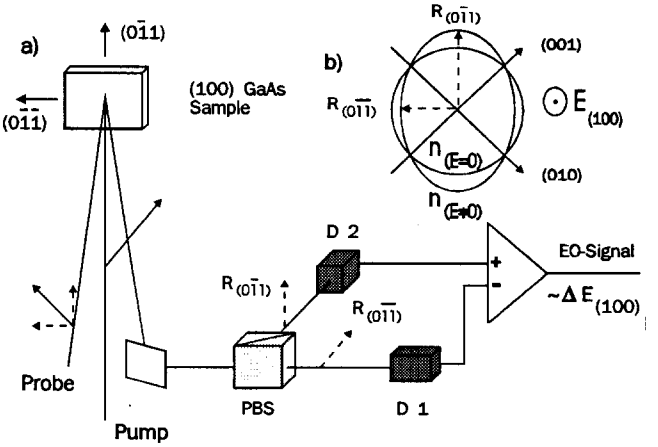


**Fig. 3. a** Optical indicatrix of (100)-oriented GaAs and **b** REOS set-up. The letters in the diagram refer to PBS: polarizing beam splitter, D1,2: photodetectors 1,2

differential detection can be described by

$$\Delta R = \Delta R|_0 + \frac{\partial \Delta R}{\partial t}\,\Delta t\,, \tag{11}$$

neglecting higher terms in $\Delta t = \Delta t_0 \sin(2\pi\nu_S t)$. Using a Lock-In amplifier with a reference frequency of $\nu_S$, the time derivative signal of $\Delta R/R_0$ is obtained. In this case the time delay between pump and probe is accomplished via a stepper-motor-driven delay stage. The sensitivity of this differential detection technique is comparable to that of the fast-scan technique.

It is important to note that the time differential technique allows time-resolved measurements of the current $J_j$ within the surface-space-charge region. Thus, the time differential REOS technique is able to supply data on microscopic details of microwave emission of photoexcited III–V-compounds, which has recently been investigated by many groups through THz experiments (see e.g., [20]). The transient photocurrent, $\partial J_j/\partial t$ in the surface-space-charge region radiates electromagnetic waves in the far infrared, which are detected with photoconductive dipole antennas. The spectral resolution is usually limited to approximately 2 THz. With the time-resolved differential REOS technique experimental data on the dynamics of photoexcited carriers are obtained with a much better temporal resolution.

## 3 Eperimental Results and Discussion

Figure 4 illustrates typical time-resolved REOS signals for highly $n$- and $p$-doped GaAs samples ($N_D = 2\times10^{18}\,\mathrm{cm}^{-3}$). The obvious opposite sign of the REOS signals for $p$- and $n$-doped GaAs follows directly from the reversed sign of the band bending. Both samples have been measured under the same experimental conditions. Zero time delay is defined by the maximum of the pump-probe cross-correlation signal

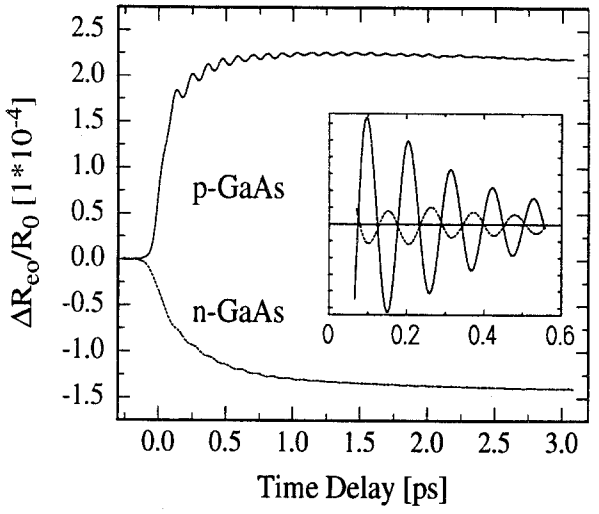


**Fig. 4.** Time-resolved REOS signals for $p$-(—)- and $n$-(- - -)-doped GaAs, especially doped with $N_D^{n,p} = 2\times10^{18}\,\mathrm{cm}^{-3}$. The inset shows the enlarged part of the phonon-induced periodic REOS modulation

obtained via two-photon absorption in GaP. The excitation density is estimated to $1\times10^{18}\,\mathrm{cm}^{-3}$.

Obviously, the REOS signals can be separated into two components. A strong positive (or negative) reflectivity change is periodically modulated by minute oscillations. The first part corresponds to transport of the photoexcited electron-hole pairs in the surface space-charge region. A very fast initial signal change is observed, which follows closely the build-up of non-equilibrium, photoexcited carriers. The signal dynamics is related to ultrafast screening of the surface field. A slower change follows, caused by the spatial redistribution of the free carriers within the surface-space-charge region. At time delays of picoseconds the field is completely screened and a near flat-band condition is approached.

Numerical simulations of the carrier dynamics have been performed based on a drift-diffusion equation. The temporal evolution of the transient electrical field is derived via Poisson's equation in a self-consistent way. Excellent agreement to the experimental data is obtained, when a saturated drift velocity of $(5\text{–}10)\times10^6$ cm/s is introduced in the simulations [21].

The period of the minute signal modulation matches exactly the frequency of the $\Gamma_{15}$-LO phonon (8.75 THz) in GaAs. In the inset of Fig. 4 the phonon-induced oscillations of $p$- and $n$-doped GaAs are shown enlarged on a time scale of 600 fs. Obviously, the phase of the oscillation is shifted by $\pi$ between the $n$- and $p$-doped sample. Both oscillatory signals can be described by an exponentially decaying cosine. This cosine behaviour indicates that the driving force is associated with the relaxation of the initial, field-induced polarization of the lattice. The initial phase (0 or $\pi$) is determined by the sign of the driving force. Remarkable differences in phonon-induced signal changes between $p$- and $n$-doped samples occur, although the static atomic displacements in both cases are comparable. The static surface fields are of comparable magnitude at equal doping densities in $p$- and $n$-doped GaAs, see (5–7). The phonon-induced REOS signal changes are, however, much larger in the case of $p$ doping. In this sample, the initial signal change (rise) is observed to be much faster than in the case of $n$ doping. This fact serves as first evidence that the amplitude of coherent phonons is determined by the time derivative of the polarization, i.e. the current density $J(t)$.

To gain more quantitative insight into the relation between phonon amplitude and the initial carrier dynamics, the screening of the electrical surface field has been modified by varying the density of photoexcited electron-hole pairs. The initial static surface-field-induced atomic displacement has been kept constant by performing the experiments on the same sample. Thus, the phonon amplitude in these experiments is only affected by the temporal variation of the longitudinal polarization due to the current surge. In Fig. 5, the time-resolved REOS signals of a $p$-doped (100)-oriented GaAs sample ($N_D = 2\times10^{18}\,\mathrm{cm}^{-3}$) are plotted for different excitation densities. The carrier density is varied over a range of two orders of magnitude by inserting neutral-density filters into the optical beam path before the pump-probe beam splitter. The initial rise in the REOS signal becomes faster with increasing carrier density. At very high photoexcited

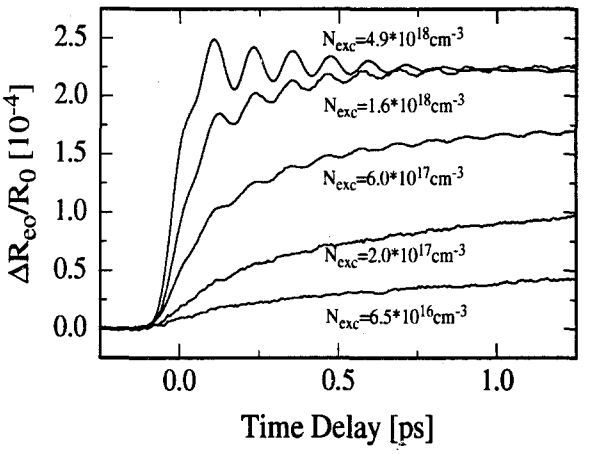


**Fig. 5.** Time-resolved REOS signals of a $p$-doped, (100)-oriented GaAs sample ($p = 2 \times 10^{18}\,\mathrm{cm}^{-3}$) as a function of photoexcited carrier density $N_{\mathrm{exc}}$

carrier densities ($N_{\mathrm{exc}} \geq 5 \times 10^{18}\,\mathrm{cm}^{-3}$) the field is completly screened within the duration of the pump pulse. At low excitation densities, however, the signal dynamics becomes more dominated by transport processes over larger distances. The amplitude of coherent phonons is, however, closely related to the magnitude of the current surge and vanishes for lower excitation densities ($N_{\mathrm{exc}} \leq 2 \times 10^{17}\,\mathrm{cm}^{-3}$), where the rise of the REOS signal is rather slow.

To clarify the exact dependence of the phonon amplitude on the initial field dynamics, the excitation density is changed in very fine steps of about 10% from $4 \times 10^{17}\,\mathrm{cm}^{-3}$ to $4 \times 10^{18}\,\mathrm{cm}^{-3}$. The experiments are performed on a specially prepared $n-(4\times10^{17}\mathrm{cm}^{-3})$-doped GaAs sample with a transparent Indium-Tin-Oxide (ITO) Schottky contact in order to apply additional internal electric fields. All experiments are performed at a fixed voltage of $U = -2\,\mathrm{V}$ in order to increase the signal dynamics. In Fig. 6a, the maximum value of the time-derived REOS signal ($(\partial\Delta R)/\partial t \sim J_j$) characterizing the initial field change due to the current surge $J_{\max}$ is plotted against the excitation density. A strictly linear relation has been found, indicating the well-known relation $J_j = qvN$ with $N = N_{\mathrm{exc}}$ and a constant drift velocity $v$, which has been found independently by the numerical simulations mentioned above [21]. The phonon induced REOS signal $\Delta R_{eo}(\omega_{\mathrm{LO}})/R_0$ is closely related to the strength of the current surge $J_{\max}$ as demonstrated in Fig. 6b. There, the oscillation amplitude is plotted versus the maximum of time-differential REOS signal. Thus the amplitude of the coherent displacement is entirely determined by the magnitude of $J(t)$.

In a complementary experiment, the influence of the initial lattice polarization is investigated. The surface fields are varied by external fields, while the carrier density is kept fixed at $5 \times 10^{17}\mathrm{cm}^{-3}$. In Fig. 7 the corresponding time-resolved REOS signals are depicted for external voltages between $+0.5\,\mathrm{V}$ to $-1.5\,\mathrm{V}$. Both, the initial rise of the REOS signals as well as the phonon signal increase with increasing electrical fields. In Fig. 8 the maximum phonon-induced signal change is plotted against the value of the initial field at zero time delay for several voltages. The

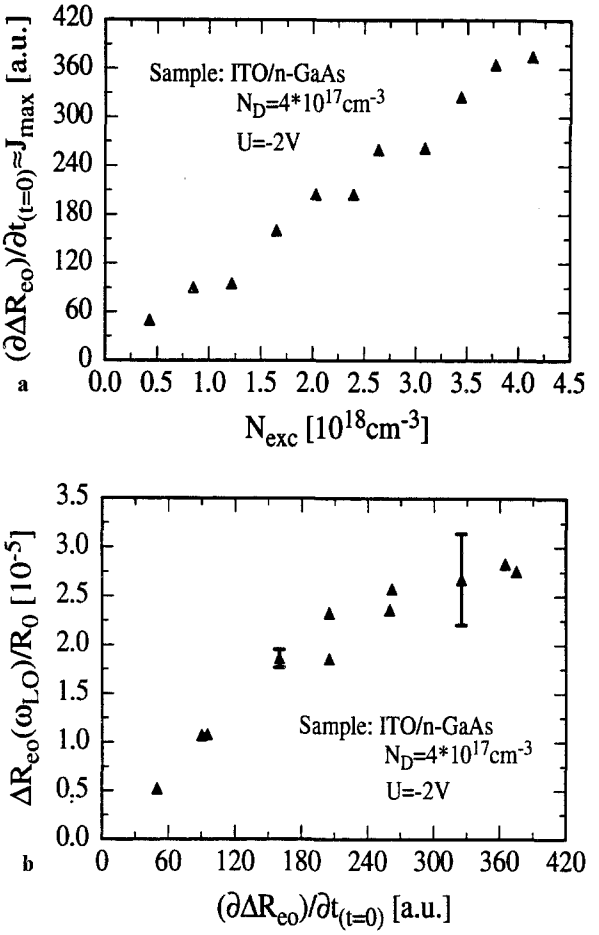


**Fig. 6.** **a** Maximum value of the time-differential REOS signal, indicating the initial field change ($\sim$ maximum value of the current $J_{\max}$) as a function of the photoexcited carrier density ($N_{\mathrm{exc}}$). **b** Phonon-induced REOS signal vs maximum value of the current ($J_{\max}$)

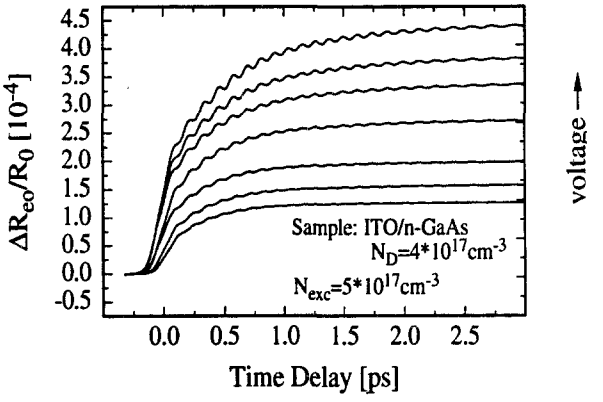


**Fig. 7.** Time-resolved REOS signals as a function of the static surface field, varied externally via a transparent ITO/$n$-GaAs Schottky contact

strictly linear relation confirms that the initial depolarization of the surface field acts as a driving force for the coherent LO phonons, and that the phonon amplitude scales with the initial static atomic displacement.

To study possible alternative generation mechanisms for coherent LO phonons, we performed a detailed study of sym-

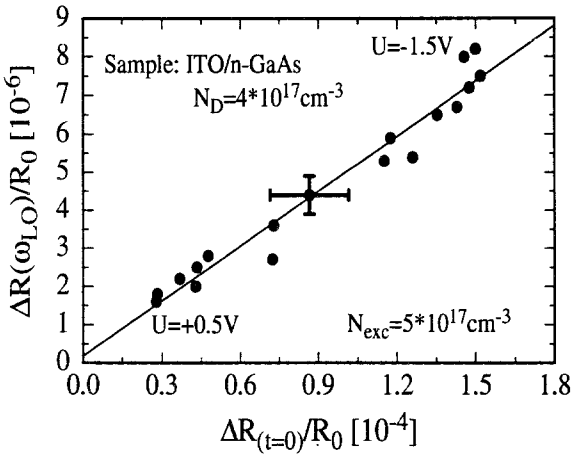


**Fig. 8.** Phonon-induced reflectivity change as a function of the REOS signal at zero time delay. The solid line is a linear fit to the measured data

metry conditions, under which coherent phonons appear. The displacement Raman term as well as the second-order nonlinear polarization require the same symmetry, i.e. the only non-zero elements are $\bar{R}_{xyz} = \bar{R}_{xzy}$. The oscillations should only appear when the pump beam is polarized along one of the (011) crystal axes. In Fig. 9 the experimentally determined time derivatives of the REOS signals are compared for two different polarizations of the pump beam, (011) and (010), which are related to the allowed and forbidden Raman excitation configurations, respectively. The polarization of the probe beam remains parallel to $(0\bar{1}0)$. Both curves are identical, aside from an additional structure in the $yz$ configuration due to a coherent artefact. Subtracting these signals gives a time derivative cross-correlation curve. The zero crossing of this curve allows the exact determination of zero time delay. It is obvious from Fig. 9 that both, phase

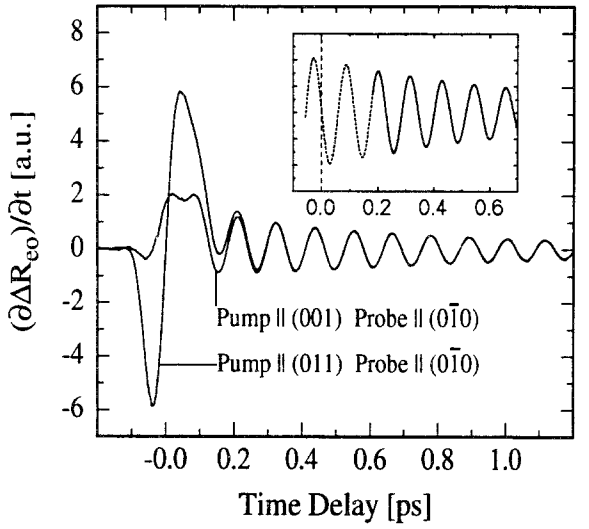


**Fig. 9.** Time differentiated REOS signals at two different polarizations of the pump beam corresponding to allowed and forbidden Raman scattering configurations, respectively. The inset shows the extracted phonon signal (—) in comparison to an exponentially decaying sine-fit (- - -)

and amplitude of the phonon oscillations, remain unchanged. This is clear evidence for a strictly isotropic generation process, contrary to what is expected from the symmetry requirements of ISRS. Furthermore, coherent oscillations induced by conventional nonresonant ISRS excitation mechanism require a $Q(t) \sim \sin(\omega_{LO}t)$ behaviour in contradiction to the experimentally observed $Q(t) \sim \cos(\omega_{LO}t)$ signal. In the inset of Fig. 9 the extracted phonon signal is illustrated together with an exponentially decaying $Q(t) \sim \sin(\omega_{LO}t)$ fit. The sine-dependence of the time derivative signal is, of course, equal to a $Q(t) \sim \cos(\omega_{LO}t)$ behaviour in the REOS signal obtained in the fast-scan mode (Fig. 4).

The only nonlinear polarization left is then of third order. The non-vanishing components in the case of $\bar{4}3m$ group elements in our experimental configuration are $xxyy = xxzz$, $xyxy = xzxz$ and $xyyx = xzzx$ [15], where the third field, along $x$, is given by the surface field. The resulting third-order nonlinear polarization is then independent of the initial polarization of the (pump)-laser fields ($xyyx = xzzx$). This Franz-Keldysh-type effect was also discussed by Gay et al. [22] as being responsible for the generation of field-induced Raman scattering (FIRS) in a number of III–V-compounds using cw lasers. The concept of polarized, intermediate excitonic states [23] has also been introduced recently, to explain details of the Far-Infrared (FIR) radiation emitted from III–V-semiconductor surfaces when irradiated with fs laser pulses. There, the emitted THz signal is explained by a third-order nonlinear polarization phenomenon, whose order is lowered to $\chi^{(2)}$ by a symmetry-breaking surface field. It is important to mention that, in contrast to their explanation and experimental findings, our experimental observations of both the surface field and the phonon-induced signal components reveal a complete isotropic behaviour (Fig. 9). Simple ultrafast drift-diffusion processes of the photoexcited carriers within the surface-space-charge region are sufficient to explain all of the experimental results presented here.

The field-induced Raman scattering (FIRS) dominates the allowed Raman scattering only, when the laser frequencies are close to electronic resonances, e.g. direct gaps [24]. In FIRS experiments at the $E_1(T = 300\,\mathrm{K}) = 2.9\,\mathrm{eV}$ resonance in (100) GaAs an extremely resonant behaviour is observed [25]. Temperature detuning of the gap by only 50 meV out of resonance to the exciting laser frequency leads to a decrease of the Raman scattering efficiency by appr. 4 decades. Thus, FIRS effects should be negligible at our laser energy of 2 eV. Temperature-dependent REOS measurements reveal no enhancement of the phonon amplitude between 4 K and 300 K, as would be expected from the temperature-induced shift of the $E_1$ and $E_0 + \Delta_0$-gap ($= 1.77\,\mathrm{eV}$ at 300 K). Furthermore, FIRS predicts an instantaneous, short-lived nonlinear polarization, with a duration comparable to the laser pulse width. Such features are not observed in our experiments.

## 4 Conclusion

Detailed investigations of the generation mechanismen of LO phonons in surface-space-charge regions have been performed in GaAs. High-sensitive, time-resolved femtosecond

pump-probe experiments allow the detection of the amplitude and the phase of coherent oscillation with high accuracy. The ultrafast screening of electrical surface fields due to ultrafast drift- and diffusion-controlled photocurrents is the main driving force for coherent LO phonons. Further possible excitation mechanisms such as the Raman process (ISRS) and a second-order nonlinear polarization are excluded by symmetry arguments. Temperature-dependent REOS measurements reveal that field-induced Raman scattering (FIRS) at the $E_1$ or the $E_0+\Delta_0$-gap can be neglected.

*Acknowledgements.* We thank A. Förster and H. Lüth (ISI, KFA Jülich) for supplying high-quality GaAs MBE samples and B. Görig (Humboldt University, Berlin) for the ITO/*n*-GaAs sample. Gratefully acknowledged are the helpful discussions with R. Scholz, A. Esser, J. Geurts (RWTH Aachen) and N. Esser (TU Berlin). This work was entirely supported by the "Deutsche Forschungsgemeinschaft" and the "Alfried Krupp" foundation.

## References

1. E.P. Ippen, C.V. Shank: In *Ultrashort Light Pulses*. ed. by S.L. Shapiro, Topics Appl. Phys. **18** (Springer, Berlin, Heidelberg 1984) Chap. 3, p. 83
2. *Ultrafast Phenomena VII*, ed. by C.B. Harris, E.P. Ippen, G.A. Mourou, A.H. Zewail (Springer, Berlin, Heidelberg 1990) Springer Ser. Chem. Phys. Vol. 53. See also earlier vols.
3. T.K. Cheng, S.D. Brorson, A.S. Kazeroonian, J.S. Moodera, G. Dresselhaus, M.S. Dresselhaus, E.P. Ippen: Appl. Phys. Lett. **57**, 1004 (1990)
   T.K. Cheng, J. Vidal, H.J. Zeiger, G. Dresselhaus, M.S. Dresselhaus, E.P. Ippen: Appl. Phys. Lett. **59**, 1923 (1991)
4. J.M. Chwalek, C. Uher, J.F. Whitaker, G.A. Mourou, J.A. Agostinelli: Appl. Phys. Lett. **58**, 980 (1991)
5. W. Kütt, W. Albrecht, H. Kurz, to be published in IEEE J. Quant. Electr. (October 1992)
6. K. Seibert, H. Heesel, W. Albrecht, J. Geurts, K. Allakhverdiev, H. Kurz: 20th Int'l Conf. on *The Physics of Semiconductors 3*, ed. by E.M. Anastassakis, J.D. Joannopoulos (World Scientific, Singapore 1990)
7. G.C. Cho, W. Kütt, H. Kurz: Phys. Rev. Lett. **65**, 764 (1990)
8. W. Kütt, G.C. Cho, T. Pfeifer, M. Strahnen, H. Kurz: Digest of CLEO (Optical Society of America, Washington, DC 1991)
9. Y.X. Yan, E.B. Gamble, K.A. Nelson: J. Chem. Phys. **83**, 5391 (1985)
10. H.J. Zeiger, J. Vidal, T.K. Cheng, E.P. Ippen, G. Dresselhaus, M.S. Dresselhaus: Phys. Rev. B **45**, 768 (1992)
11. T. Pfeifer, R. Scholz, W, Kütt, H. Kurz: Submitted to Phys. Rev. Lett.
12. L. Min, R.J.D. Miller: Appl. Phys. Lett. **56**, 524 (1990)
13. W. Kütt, G.C. Cho, M. Strahnen, H. Kurz: Appl. Surf. Sci. **50**, 325 (1990)
14. W.E. Bron, J. Kuhl, B.K. Rhee: Phys. Rev. B **34**, 6961 (1986)
15. Y.R. Shen: *The Principles of Nonlinear Optics* (Wiley, New York 1984)
    D.L. Mills: *Nonlinear Optics* (Springer, Berlin, Heidelberg 1991)
    V.G. Dmitriev, G.G. Gurzadyn, D.N. Nikogosyan: *Handbook of Nonlinear Optical Crystals*, Springer Ser. Opt. Sci., Vol. 64 (Springer, Berlin, Heidelberg 1991)
16. W.E. Spicer, I. Lindau, P. Skeath, C.Y. Yu, P. Chye: Phys. Rev. Lett. **44**, 420 (1980)
17. C.C. Shih, A. Yariv: J. Phys. C **15**, 825–846 (1982)
18. M. Strahnen, W. Kütt, H. Kurz: In *Proc. Int'l Conf. on VME-bus in Research*, ed. by C. Eck (North-Holland, Amsterdam 1988) p. 69
19. J. Chesnoy, A. Mokhtari: Rev. Appl. Phys. **22**, 1743 (1987)
20. X.C. Zhang, D.H. Auston: J. Appl. Phys. **71**, 326 (1992)
21. T. Dekorsy, T. Pfeifer, W. Kütt, H. Kurz: Submitted to Phys. Rev. B
22. J.G. Gay, J.D. Dow, E. Burstein, A. Pinzcuk: In *Light Scattering in Solids*, ed. by M. Balkanski (Flammarion, Paris 1971) p. 33
23. S.L. Chuang, S. Schmitt-Rink, B.I. Greene, P.N.. Saeta, A.F.J. Levi: Phys. Rev. Lett. **68**, 102 (1991)
24. W. Richter: In *Solid State Physics* Springer Tracts in Modern Physics, Vol. 78 (Springer, Berlin, Heidelberg 1976)
25. N. Esser: Institute of Solid State Physics, TU Berlin (private communication)